Acoustic scattering by multicracks using a boundary finite element method

Carlos J. S. Alves

CEMAT - Department of Mathematics, Instituto Superior Técnico
Av. Rovisco Pais 1, 1049-001 Lisboa, Portugal
e-mail: Carlos.Alves@math.ist.utl.pt

Keywords: Boundary Element Method, Finite Elements, Acoustic Scattering, Crack Detection, Multicracks.

Abstract. The numerical simulation of crack scattering is an exterior problem where the use of boundary element methods is recommended. However when considering Neumann boundary conditions in the crack, difficulties connected to the hypersingularity in double layer potential kernel arise. The use of a boundary variational formulation on the boundary allows to overcome this difficulties. This was introduced in Nédélec [14] for the Laplace equation, and developed by Hamdi [9] for the case of acoustic scattering. The case of flat cracks has been addressed by Ha Duong [8]. In the case of a single flat cracks this method has been has been applied [1] with robust results also in the elastic crack scattering framework. In [3] the method was extended to non-planar cracks and here we present the multicrack case, showing simulations for the convergence of the method and we discuss some results concerning crack identification.

Introduction

The numerical simulation of acoustic and elastic scattering by cracks has been associated with several applications, namely the control and detection of imperfections in some materials. Some of the first numerical studies considered scattering by flat simple shaped cracks, such as the penny-shaped crack (eg. Bouwkamp [6], Jones [11]), where a solution was possible using special coordinate systems. This exterior problem was suitable to boundary element method approach, but it had a major difficulty arising from the hypersigularity in the kernel of the associated first kind boundary integral equation. The integral could only be defined in a weak sense and some of the first successful methods used a truncated series expansion (cf. [12]). More recently some techniques with regularization have been applied to the standard collocation boundary element method (eg. [5], [13]). On the other hand, since the works of Nédélec [14] and [10] the introduction of a finite element method associated to the variational formulation of the boundary integral equation gave new possibilites to the boundary element method. This technique has been applied in the case of acoustic scattering (cf. Hamdi [9]), and in the particular case of plane cracks coercivity was proven (cf. Ha Duong [8]). The numerical simulation for acoustic and elastic plane flat cracks was presented in [1], showing the good performance of this technique compared to previous ones. In [3] simulations for the more general case of acoustic scattering by a non flat crack have been presented. In this work we show some numerical simulations applying the method to multicracks, analysing the convergence of the method and presenting some preliminary simulations that may lead to criteria showing the influence of the multicrack framework on crack detection as in [2].

Acoustic Scattering by Cracks

We consider the general setting for time-harmonic acoustic scattering by cracks, which is modelled by the Helmholtz equation, and we will be mainly interested in wavelenghts that are comparable to the dimensions of the crack. Scattering models for short or long wavelengths can be simpler using asymptotic expansions (e.g. [4]). We will denote by Γ the set of c surfaces describing the cracks $\Gamma_1, ..., \Gamma_c$, each one considered as a part of regular boundary (piecewise C^1) of a bounded domain of $\mathbb{R}^3$. Thus, the set Γ has c connected components, each surface describing a crack, and we assume that each surface is orientable, excluding not only some exhotic surfaces like the Möbius strip, but also crack bifurcations.
In the homogeneous medium we assume that the constant propagation speed is unitary, and therefore the wavenumber $k > 0$ coincides with the frequency.
The amplitude of the scattered wave u verifies the Helmholtz equation in the domain $\mathbb{R}^3 \setminus \Gamma$,

$$\Delta u + k^2 u = 0 \quad \text{in } \mathbb{R}^3 \setminus \Gamma$$

and on the crack surface the Neumann boundary condition is considered,

$$\partial_n u = -\partial_n u^{inc} \quad \text{on } \Gamma.$$

Here will be mainly interested in plane incident waves

$$u^{inc}(x) = e^{ikx\cdot d},$$

with propagation direction $d \in S^2$ (here S^2 represents the unitary sphere).
Thus we obtain the following problem

$$\begin{cases} \Delta u + k^2 u = 0 & \text{in } \mathbb{R}^3 \setminus (\bigcup_{m=1}^{c} \Gamma_m) \\ \partial_n u = -\partial_n u^{inc} & \text{on } \Gamma \\ \partial_r u - iku = o(r^{-1}) & \text{when } r = |x| \to \infty, \end{cases}$$

where the last condition is the *Sommerfeld radiation condition*, that allows to establish the uniqueness of the problem. This a well posed problem (cf. [7]) and furthermore the asymptotic behavior of the scattered wave can be described by the relation

$$u(x) = \frac{e^{ikr}}{r} u_\infty(\hat{x}) + o(\frac{1}{r}),$$

where $\hat{x} = \frac{x}{|x|} \in S^2$, and u_∞ is an analytic function on S^2, known as the *far field*. The far field determines completely the scattered wave (a Theorem by Rellich).
We consider the multicrack framework where $\Gamma = \Gamma_1 \cup \cdots \cup \Gamma_c$, and each Γ_m is a connected component of Γ. The solution of this problem can be described through the double layer potential (e.g. [8])

$$\begin{aligned} u(x) &= \int_\Gamma \partial_{n_y} \Phi(x-y)\varphi(y) ds_y, \quad (x \in \mathbb{R}^3 \setminus \Gamma) \\ &= \sum_{m=1}^{c} \int_{\Gamma_m} \partial_{n_y} \Phi(x-y)\varphi_m(y) ds_y \end{aligned} \tag{1}$$

where Φ is the 3D fundamental solution of the Helmholtz equation, given by

$$\Phi(x) = \frac{e^{ik|x|}}{4\pi|x|}, \quad \text{with } |x|^2 = x_1^2 + x_2^2 + x_3^2$$

where $\varphi_m \in H_{00}^{1/2}(\Gamma_m)$ is a density function determining the jump in the crack Γ_m known as the *crack opening displacement*. The jump is defined by the difference between the two traces of the solution in Γ_m, that is, $\varphi = [u] = u^- - u^+$.
On the other hand, the normal trace of the double layer potential is given by

$$-\partial_{n_x} u^{inc}(x) = \partial_{n_x} \int_\Gamma \partial_{n_y} \Phi(x-y)\varphi(y) ds_y, \tag{2}$$

leading to an integral equation of the first kind. The boundary element method presents now a difficulty related to the hypersingularity in the integral kernel, since

$$\partial_{n_x}\partial_{n_y} \Phi(x-y) = O(\frac{1}{|x-y|^3})$$

is not integrable in the usual sense.
The boundary variational formulation obtained by Hamdi (cf. [9]) is now applied to non planar cracks. The variational problem consists in the determination of the density function $\varphi \in H_{00}^{1/2}(\Gamma)$ such that

$$\begin{aligned} \int_\Gamma \int_\Gamma \Phi(x-y) \big(&\mathbf{rot}_\Gamma \varphi(x) \cdot \mathbf{rot}_\Gamma \bar{\psi}(y) - \\ &- k^2 \mathbf{n}_x(x) \cdot \mathbf{n}_y(y) \varphi(x) \bar{\psi}(y) \big) ds_y ds_x = -\int_\Gamma \partial_n u^{inc}(x) \bar{\psi}(x) ds_x, \end{aligned} \tag{3}$$

for any test function $\psi \in H_{00}^{1/2}(\Gamma)$. The differential operator $\mathbf{rot}_\Gamma$ is the surface rotational given by

$$\mathbf{rot}_\Gamma \varphi(x) = \mathbf{n}_x \times \nabla \tilde{\varphi}(x).$$

This way we circumvent the problem of integrating an hypersingular kernel, since the double derivation of the kernel given by the fundamental solution $\Phi(x-y)$ is transferred in the weak formulation to the derivative of the crack opening displacement density and to the derivative of the test function.

Boundary Finite Element Method

The boundary finite element method combines the discretization with boundary elements with the finite element approach. We will use $\mathcal{P}_1$ basis functions defined on those boundary elements. The greater difficulty of the method consists in the approximation of the double integration since the kernel defined by the fundamental solution remains weakly singular.

In the case of multicracks $\Gamma = \Gamma_1 \cup \cdots \cup \Gamma_c$, each of the surfaces Γ_m will be represented by the graph of a function f_m defined on plane surface Q_m (for instances, an $\mathbb{R}^2$ rectangle), that is $\Gamma_m = f_m(Q_m)$,

$$\Gamma_m = \{(x^*, f_m(x^*)),\ \text{com}\ x^* \in Q_m \subset \mathbb{R}^2\}.$$

The regularity of the function f estabishes the regularity of the surface Γ_m. Then each surface Γ_m is discretized with triangles

$$T_k = \bigcup_{i=1}^{3} (x_{k_i}^*,\ f_m(x_{k_i}^*))$$

where $x_{k_i}^*$ are points in a bidimensional mesh defined on Q_m, and k_i is a representation of the node i of the triangle k in the global numeration.
With this procedure the multicrack is approximated by the union of piecewise triangular cracks, ie. $\Gamma_h = \cup_k T_k$ approximates Γ, denoting h the diameter of the triangles T_k. One should notice that the meshes of Q_m do not transfer directly their properties to the discretized surface $\tilde{\Gamma}_m$. For instance, a function f_m with high gradient might transform a triangle τ_k on Q_m into an almost degenerated triangle $T_k = f_m(\tau_k)$.
Associated to the triangulation we consider Lagrange finite elements $\mathcal{P}_1$ vanishing on the border of each Γ_m, which is an appropriated continuous approximation $\varphi_m \in H_{00}^{1/2}(\Gamma_m)$,

$$H_{00}^{1/2}(\Gamma_m) = \{\phi \in H^{1/2}(\Gamma_m) : \rho^{-1/2}\phi \in L^2(\Gamma_m)\}.$$

where ρ is equivalent to the distance to the border, ie. $\text{dist}(\cdot, \partial\Gamma)$. In Fig. 1 we present an example of triangulation for a double crack with non planar components. The triangulation is made in such a way that each interior node is associated with six adjacent triangles.
Having obtained the mesh we calculate the double integral in the sesquilinear form as the sum of double integrations over the element triangles, taking into account two different situations:

(i) Non adjacent triangles $\longmapsto$ we consider numerical integration for both integrals using interior Gauss points.

(ii) Adjacent triangles $\longmapsto$ we conside numerical integration in the first integral on a triangle T_i and for each Gauss point y_g we need to consider an analytical integration (cf. [1])

$$\int_{T_j} \Phi(x-y_g)\,(\mathbf{rot}_\Gamma \varphi(x) \cdot \mathbf{rot}_\Gamma \bar{\psi}(y_g) - k^2 \mathbf{n}_x(x) \cdot \mathbf{n}_y(y_g)\varphi(x)\bar{\psi}(y_g))\,ds_x.$$

Note that φ and ψ basis functions of the discrete space. Since we consider interior Gauss points, there are only integration singularities when $T_i = T_j$. In the other situations we may proceed with numerical integration. The analytic calculation of the integral is what consumes most part of the computational time.

Through the resolution of the linear system associated to the discretization of the variational formulation, we obtain coefficients that define the aproximation of φ as a linear combination of the basis functions. This way we may calculate an approximation of the far field amplitude through the formula

$$u_\infty(\hat{x}) = \frac{1}{4\pi} \sum_{m=1}^{c} \int_{\Gamma_m} \partial_{n_y} e^{-ik\hat{x}.y} \varphi_m(y) ds_y,$$

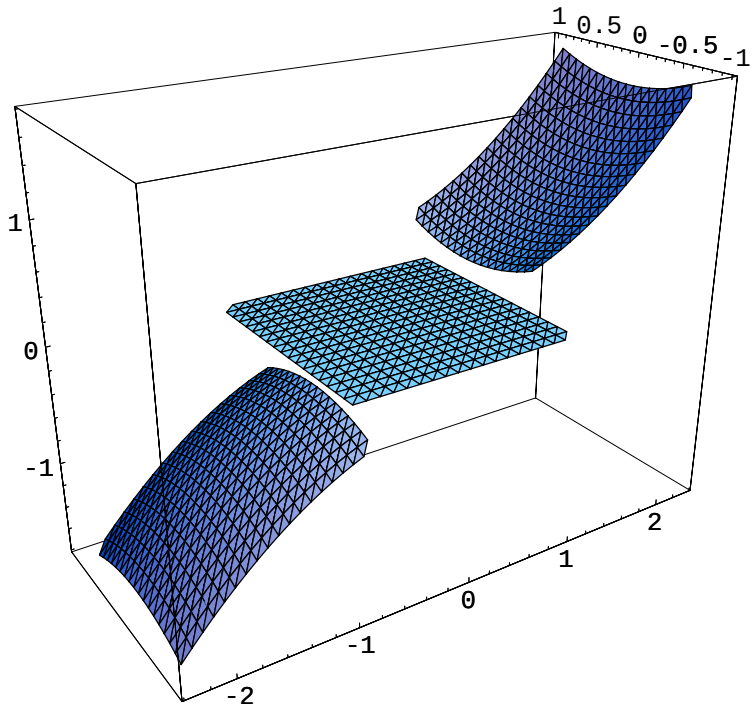

Figure 1: A mesh with 49 interior nodes, for each one of the three cracks.

using the integration rule with the Gauss points defined in each triangle approximating Γ_m.

Error Estimate
In $H_{00}^{1/2}(\Gamma)$ the norm is defined by

$$||\phi||^2_{1/2,00} = ||\phi||^2_{1/2} + ||\rho^{-1/2}\phi||^2_0$$

and in the plane crack case we may establish an $O(h^{3/2})$ convergence using Lagrange finite elements $\mathcal{P}_1$.
In fact, considering a triangulation $\mathcal{T}_h$, let Π_h be the projection operator in the finite dimensional space defined by Lagrange finite elements of order k. Thus, $\Pi_h\phi$ is the interpolating function for $\phi \in H^{k+1}(\Gamma)$, and applying an interpolation inequality between $L^2 = H^0$ and H^1 Sobolev spaces we get

$$||\phi - \Pi_h\phi||^2_{1/2} \leq C||\phi - \Pi_h\phi||_0||\phi - \Pi_h\phi||_1.$$

Using the interpolation estimates for Lagrange finite elements of order k

$$||\phi - \Pi_h\phi||_0 \leq Ch^{k+1}||\phi||_{k+1}, \quad ||\phi - \Pi_h\phi||_1 \leq Ch^k||\phi||_{k+1},$$

we derive the estimate

$$||\phi - \Pi_h\phi||_{1/2} \leq Ch^{k+1/2}||\phi||_{k+1}.$$

In our case, since we are using $\mathcal{P}_1$ finite elements then $k = 1$, and without going through more technical details, this partially justifies the $O(h^{3/2})$ rate of convergence, when we have a regular setting and $\varphi \in H^2$, in particular for plane incident waves. This rate of convergence obtained for the density is then inherited by the calculations of the far field amplitude.
In the non planar crack case, such rate of convergence is diminished by the geometry approximation, since we are approaching the regular surfaces by piecewise triangular surfaces. Thus can expect a decrease of about $\frac{1}{2}$ in the convergence order, leading to an $O(h)$ approximation.

Numerical Simulations

We first present some numerical simulations concerning the convergence rate of the method. Calling $F(h)$ the evaluated far field amplitude with an h size mesh, the rate of convergence is evaluated numerically using three tests, using different h_{n-1}, h_n, h_{n+1}. Assuming that $E(h) = F - F(h) \approx Ch^p$, we obtain a value p approximated by p_n, the solution of the nonlinear equation

$$\frac{||F(h_{n-1}) - F(h_n)||}{||F(h_n) - F(h_{n+1}||} = \frac{h_{n-1}^{p_n} - h_n^{p_n}}{h_n^{p_n} - h_{n+1}^{p_n}} \tag{4}$$

and we obtain an approximated C by the value

$$C_n = \frac{||F(h_{n-1}) - F(h_n)||}{h_{n-1}^{p_n} - h_n^{p_n}}. \tag{5}$$

As a test we considered a plane wave with direction $d = (0,0,-1)$, frequency $k = 2$ incident on three cracks, two of them not flat, as shown in Fig. 1. The cracks Γ_m are obtained as the graphs of $f_m(x,y) = (m-2)\frac{1}{4}(1 + x^2 + y^2)$, for $(x,y) \in \alpha_m Q_m$ with $Q_m = [\frac{3}{2}(m-2) - 1, \frac{3}{2}(m-2) + 1] \times [-1,1]$ and $\alpha_1 = \alpha_3 = 0.8, \alpha_2 = 1$.

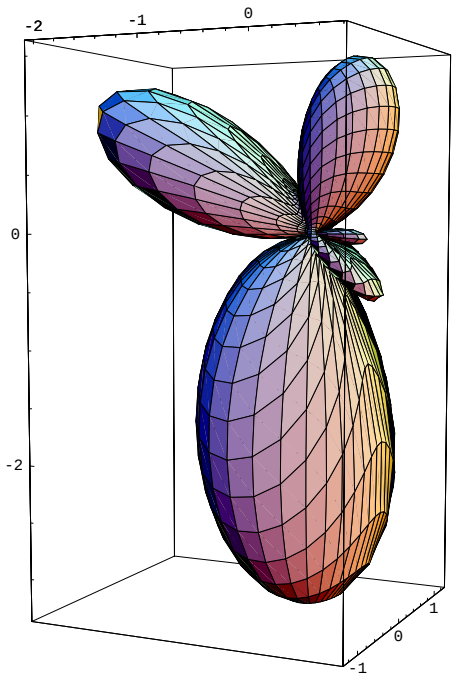

Figure 2: Modulus of the far field pattern generated by the 3 cracks with $d = (0,0,-1)$ and $k = 2$.

The 3D plot of the far field modulus is presented in Fig. 2, and in Fig. 3 we present a cut of the 3D plots showing the convergence pattern using $M = 36$ observation points. Using those values, we obtained the estimates in Table 1.

Table 1. Convergence results.

n	h_n^Q	N	h_n	$\|\|F(h_n)\|\|_\infty$	$\frac{1}{M}\|\|F(h_n) - F(h_{n+1})\|\|_{l^2}$	p_n	C_n
1	0.5	26	0.782049	2.65687	0.0301858		
2	0.3333	74	0.533796	2.95359	0.0124467	1.680	0.947
3	0.25	146	0.405093	3.07630	0.00683649	1.432	0.923
4	0.2	242	0.326373	3.14346	0.00434551	1.301	0.888
5	0.1667	362	0.273261	3.18596	0.00301303	1.230	0.858
6	0.1429	506	0.235013	3.21532	0.00221712	1.177	0.831
7	0.125	674	0.206155	3.23685	0.00170128	1.146	0.812
8	0.1111	866	0.183609	3.25332			

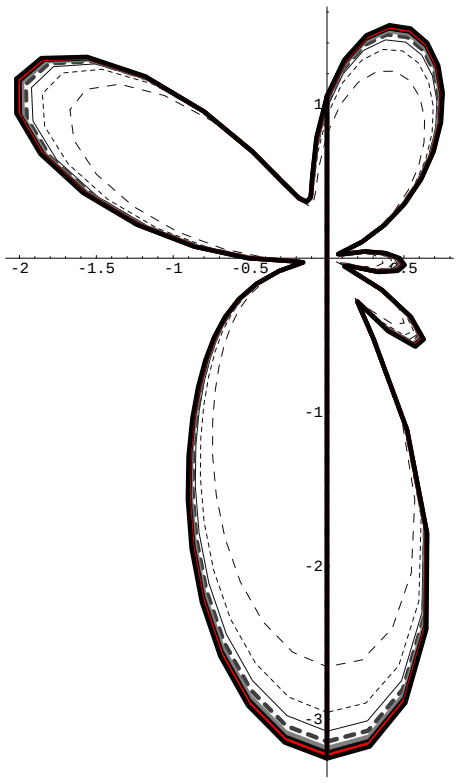

Figure 3: Convergence of the far field modulus (cuts of the 3D pattern for several h).

In Table 1 we present the results for several meshes, with h_n^Q representing the step size on each square Q_m that leads to a mesh discretization of Γ_m with diameter h_n (fourth column). The number N represents the number of interior nodes and therefore the dimension of the rigid matrix $N \times N$. In the fifth column we see the convergence of the far field values $||F(h_n)||_\infty = \max_{j=1,\ldots,M} |\tilde{u}_\infty(d_j)|$, where d_j represent the $M = 36$ equally angular spaced observation directions, and $|\tilde{u}_\infty(d_j)|$ the far field modulus taken on a cut of the sphere (as presented in Fig. 2).
In the next column we show the l^2 average of the the difference between two successive mesh sizes, ie. $\frac{1}{M}||F(h_n) - F(h_{n+1})||_{l^2}$ and in the other two columns we present the instant estimate of the rate of convergence p_n as given by eq.(4) and C_n as given by eq.(5).
It is worth noting that the convergence rate becomes close to 1 as predicted in the error estimate section. It starts closer to 1.5 but it decreases almost to 1, revealing the effect of the geometry approximation (piecewise triangular shape) in decreasing the convergence rate.
On the other hand, as we may see in Fig. 2, where we plotted the curves from $n = 1$ (dashed) to $n = 8$ (bold), the general aspect of the far field pattern is obtained even with considerably large h_n. In fact already with h_4 it becomes to difficult to see a difference with the results produced by the smaller h_8. Since for h_8 we need to compute the integrals for a 866×866 matrix, against a 242×242 matrix with h_4, there is no significant advantage in the given example to consider higher approximations. We should note however that the results became worst when the frequency is higher and also when we are dealing with more complex crack shapes. In those situations a smaller h must be considered.

In the next simulations, keeping the plane crack Γ_2 fixed, we show the influence on the far field of the growing area of the other two cracks, by increasing the parameter $\alpha_1 = \alpha_3 = \alpha$ from 0 to 1 (recall that this parameter defines the support of the graph). The case $\alpha = 0$ corresponds to consider only the flat crack Γ_2.
In Fig.4 we show the far field patterns obtained for $\alpha = 0.01, 0.4, 0.6$. (from left to right). In this three simulations, the effect of the small cracks Γ_1 and Γ_3 becomes only clearly noticed with $\alpha = 0.6$, where a new lob is starting to be formed.
The effect of the Γ_1 and Γ_3 becomes clear when we increase α to 0.8 or to 1.0, as we may see in Fig. 5 (center and right). In this situation the far field pattern can be seen as a mixture of the far field obtained for an oblique plane crack with $f_2(x) = x_1$, (Fig.5 - left) and the far field obtained for $f_2(x) = 0$ (Fig. 4 - left).

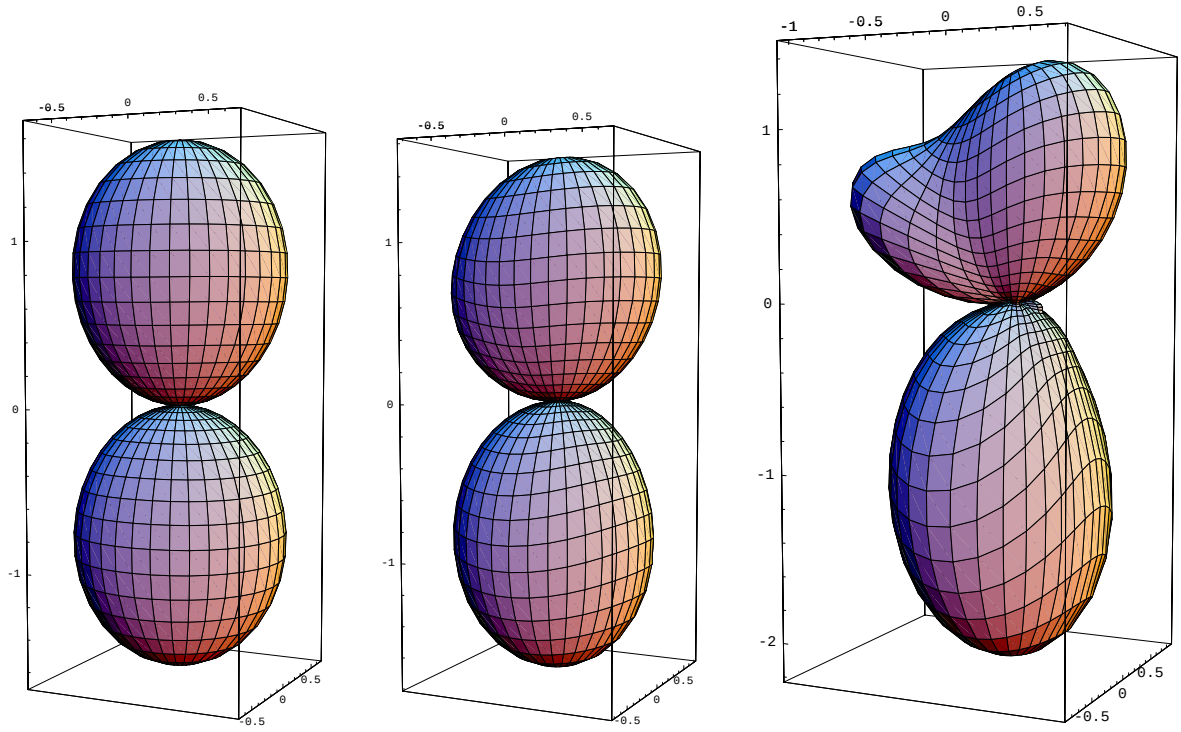

Figure 4: Far field modulus increasing $\alpha = 0.01, 0.4, 0.6$ (from left to right).

When α increases the overall shape of the three cracks can be roughly approximated by the oblique crack. This roughly justifies the increase of the contribution of the corresponding reflection lobs of the oblique crack and the decrease of the contribution given by the *horizontal* crack Γ_2.

Conclusions

In this work we have shown that the boundary finite element method provides good approximations of the scattered field by several cracks. We have presented several numerical simulations confirming the expected rate of convergence, and aiming detection criteria, we started to investigate the effect on the far field generated by the presence of other cracks. It was also observed that this method is not adequate if we consider a significant number of cracks, since there will be a compromise between the precision and computational time required by an extensive meshing. However, it was noticed that the method presented good results even with a small number of interior nodes. A more careful study on the difference between the total scattering and the sum of independent scatterers may provide criteria for crack detection.

Acknowledgements. This work is partially supported by FCT through the program POCTI-FEDER and project POCTI/MAT/34735/2000.

References

[1] C.J.S. Alves and T. Ha Duong, Numerical resolution of the boundary integral equations for elastic scattering by a plane crack, *Int J. Num. Meth. Eng.*, **38**, pp.2347–2371 (1995).

[2] C.J.S. Alves and T. Ha Duong, On inverse scattering by screens, *Inverse Problems*, **13**, pp.1161–1176 (1997).

[3] C.J.S. Alves, B. Pereira and P. Serranho, Scattering by cracks: Numerical simulations using a boundary finite element method, in *Boundary Elements XXIV* (Ed: C. A. Brebbia, A. Tadeu, V. Popov), WIT Press, pp. 35-44 (2002).

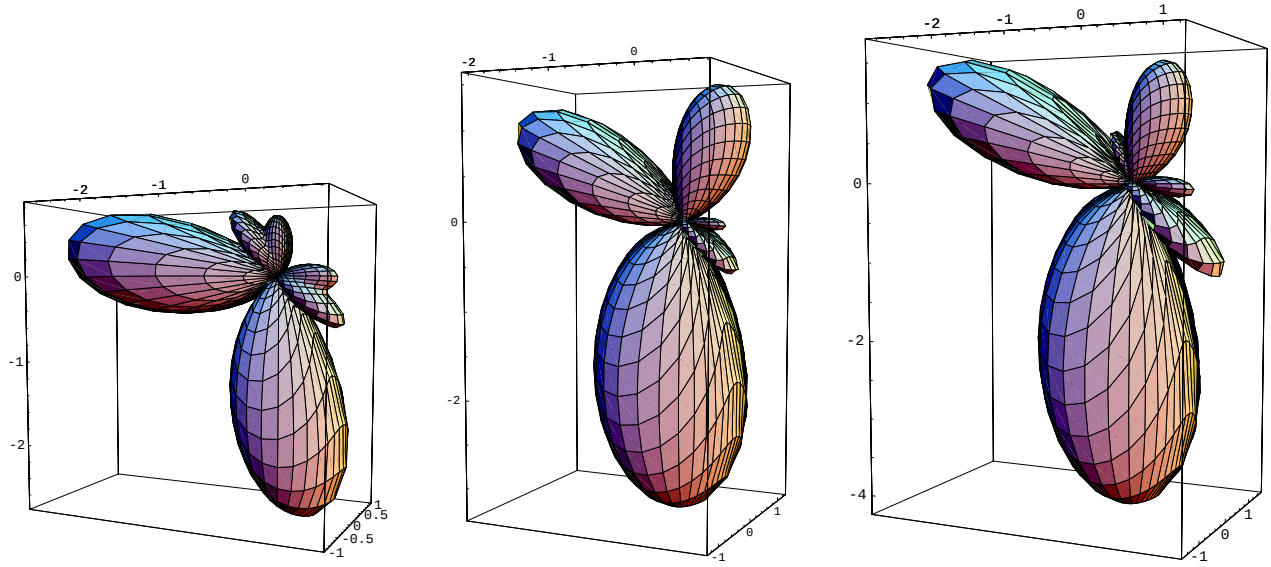

Figure 5: Far field modulus for an oblique plane crack (left) and with $\alpha = 0.8, 1.0$. (center and right)

[4] H. Ammari and P. Ferreira, Numerical methods for the scattering by gratings at high frequencies. *Math. Meth. Appl. Sci.* **20** , pp. 1531-1549 (1997).

[5] M. Bonnet, Regularized BIE formulations for first- and second-order shape sensitivity of elastic fields. *Comput. & Structures* **56,** pp.799–811 (1995).

[6] C.J. Bouwkamp, Diffraction theory. *Reports on Progress in Physics* **17**, pp.35–100, (1954).

[7] D. Colton and R. Kress, *Inverse acoustic and electromagnetic scattering theory*, Springer-Verlag, 2nd. ed. (1998).

[8] T. Ha Duong, On the boundary integral equations for the crack opening displacement of flat cracks, *Int. Eq. Op. Th.*, pp.427-453 (1992).

[9] M.A. Hamdi, Une formulation variationnelle par équations intégrales pour la résolution de l'équation de Helmholtz avec des conditions aux limites mixtes, *C.R.A.S.*II **292**, pp.17–20, (1981).

[10] C. Johnson and J.C. Nédélec, On the coupling of boundary integral and finite element methods, *Math. Comp.* **35**, 1063 –1079 (1980).

[11] D.S. Jones, A new method for calculating scattering with particular reference to the circular disc. *Comm. Pure Appl. Math.* **9**, pp.713–746, (1956).

[12] P.A. Martin and G.R. Wickham, Diffraction of elastic waves by a penny-shaped crack: analytical and numerical results. *Proc. Roy. Soc. Lond.,* **A 390**, pp 91–129 (1983).

[13] P.A. Martin and F.J. Rizzo, On boundary integral equations for crack problems. *Proc. Roy. Soc. Lond.*, **A 421**, pp.341–355, (1989).

[14] J. C. Nedelec, Curved finite element methods for the solution of singular integral equations on surfaces in $\mathbb{R}^3$. *Comput. Methods Appl. Mech. Engrg.* **9**, 191-216 (1977).

[15] F. Penzel, Mixed Fourier boundary element methods for computing time-harmonic scattering fields on screens, *Math. Nachr.* **175,** pp.269–324, (1995).